Ocean Sci. J. (2018) 53(1):1–16
http://dx.doi.org/10.1007/s12601-017-0058-8

Article

Available online at http://link.springer.com
SpringerLink

Ocean Science Journal
pISSN 1738-5261
eISSN 2005-7172

# Interannual Variation of Surface Circulation in the Japan/East Sea due to External Forcings and Intrinsic Variability

**Byoung-Ju Choi[1,2]*, Seong Hun Cho[2], Hee Seok Jung[3], Sang-Ho Lee[2], Do-Seong Byun[4], and Kyungman Kwon[2]**

[1]*Department of Oceanography, College of Natural Science, Chonnam National University, Gwangju 61186, Korea*
[2]*Department of Oceanography, Graduate School, Kunsan National University, Gunsan 54150, Korea*
[3]*Ocean Circulation and Climate Research Center, KIOST, Ansan 15627, Korea*
[4]*Ocean Research Division, Korea Hydrographic and Oceanographic Agency, Busan 49111, Korea*

Received 25 April 2017; Revised 14 August 2017; Accepted 20 August 2017


**Abstract** – The interannual variation of surface ocean currents can be as large as seasonal variation in the Japan/East Sea (JES). To identify the major factors that cause such interannual variability of surface ocean circulation in the JES, surface circulation was simulated from 1998 to 2009 using a three-dimensional model. Contributions of atmospheric forcing (ATM), open boundary data (OBC), and intrinsic variability (ITV) of the surface flow in the JES on the interannual variability of surface ocean circulation were separately examined using numerical simulations. Variability in surface circulation was quantified in terms of variance in sea surface height, 100-m depth water temperature, and surface currents. ITV was found to be the dominant factor that induced interannual variabilities of surface circulation, the main path of the East Korea Warm Current (EKWC), and surface kinetic energy on a time scale of 2–4 years. OBC and ATM were secondary factors contributing to the interannual variation of surface circulation. Interannual variation of ATM changed the separation latitude of EKWC and increased the variability of surface circulation in the Ulleung Basin. Interannual variation of OBC enhanced low-frequency changes in surface circulation and eddies in the Yamato Basin. It also modulated basin-wide uniform oscillations of sea level. This study suggests that precise estimation of initial conditions using data assimilation is essential for long-term prediction of surface circulation in the JES.

**Keywords** – intrinsic variability, East Korea Warm Current, interannual variation, Japan/East Sea

## 1. Introduction

Ocean circulation has been considered to be significantly controlled or even determined by atmospheric forcing and open boundary data. A lot of effort has been invested in enhancing the quality of atmospheric forcing and open boundary data to improve regional ocean modeling. The predictability of regional ocean circulation is known to be limited by significant uncertainty in atmospheric forcing and open boundary data (Condron and Renfrew 2013; Meinvielle et al. 2013). Recently, the intrinsic variability of the ocean and atmosphere has been found to be an important process that induces low-frequency interannual variability (Jiang et al. 1995; Sérazin et al. 2015; Nonaka et al. 2016; Wolfe et al. 2017). There is still much uncertainty regarding extratropical ocean circulation due to its intrinsic variability, which limits the potential predictability of interannual variability along strong western boundary currents and mesoscale oceanic eddy activity such as the Kuroshio and its eastward extension (Nonaka et al. 2016). This intrinsic variability also limits the potential predictability of interannual variability in the Kuroshio Extension jet speed because the magnitude of the intrinsic variability is comparable to that of the deterministic wind-driven interannual variability.

Quasi-biennial variability of sea surface height (SSH) was observed in the Yamato Basin of the Japan/East Sea (JES) based on satellite altimeter observation and a data assimilative model simulation (Hirose and Ostrovskii 2000). Analysis of monthly sea level data at Ulleung Island from 1979 to 1992 revealed that interannual variation, intra-seasonal variability, and mean seasonal cycle account for 13%, 30%, and 54%, respectively, of monthly sea level variations (Kim et al. 2002). Empirical Orthogonal Function (EOF) analysis of the SSH obtained from satellite altimeter observation showed that

*Corresponding author. E-mail: bchoi@jnu.ac.kr

the first mode was related to uniform basin-wide oscillations over the entire JES and the second mode was associated with the interannual path change of the East Korea Warm Current (EKWC) (Choi et al. 2004). EOF analysis of the sea surface geostrophic currents estimated from satellite altimeter data for 16 years showed intensification of the EKWC along the east coast of Korea and modulation of clockwise circulation in the Yamato Basin in the first mode and meandering of the EKWC in the second mode (Choi et al. 2012). Therefore, both the first and the second modes are associated with interannual variations of the surface currents in the JES. Interannual variability of the surface ocean circulation in the JES has been thought to be related to the interannual variability of atmospheric forcing or open boundary data (Lee et al. 2010; Choi et al. 2009). However, not much attention has been given to internally generated variability due to nonlinearity of surface flow in the JES.

The following three factors have been put forward to explain how interannual variation of the EKWC in the JES is induced: (1) instability of the EKWC, (2) inflow-outflow variability, and (3) interannual changes in wind stress and winter cooling (Holloway et al. 1995; Lee 1999; Hogan and Hurlburt 2005; Lee et al. 2010; Choi et al. 2009). Holloway et al. (1995) used both mean seasonal forcing and steady forcing in a three-dimensional model with a coarse (22 km) horizontal grid spacing and found relatively large interannual variations in kinetic energy and surface circulation based on simulations of steady forcing. Lee (1999) studied interannual variation of the EKWC using a quasi-geostrophic model and concluded that barotropic instability could induce internally the interannual variation. Lee and Niiler (2010) suggested that surface circulation patterns of Ulleung Basin depend on the initial relative vorticity of the inflow through the western channel of the Korea Strait based on EOF analysis of nonseasonal sea level anomalies and patterns of surface drifter trajectories. Choi et al. (2009) used a two-dimensional reduced gravity model to identify the major factor that induces the interannual variability of the Polar Front in the JES and claimed that wind stress variability was related to that of the Polar Front. However, Lee (1999) and Choi et al. (2009) could not quantify the contribution of the internally generated variability and the interannual variations of open boundary data and atmospheric forcing to the interannual variation of the EKWC path change because they only performed simple idealized model simulations.

Interannual variations in SSH and in meridional positions of the Polar Front are as large as seasonal variations in the JES. However, quantitative estimation of the relative contributions of these factors to interannual variations in surface circulation and EKWC path has not been made in previous studies. In this paper, the relative contribution of external forcing (such as inflow transport through the narrow straits and wind forcing) and intrinsic (internally generated) variability to the interannual variability of the surface circulation is quantitatively estimated using simulations of three-dimensional ocean circulation in the JES. Numerical model configuration and experiment design are described in section 2. Variability of SSH, 100-m depth currents and temperature, EKWC path, and surface kinetic energy are estimated to find the major responsible factor in section 3. Spatial and temporal structures of the interannual variability are discussed in section 4. Results are briefly summarized in section 5.

## 2. Numerical Model and Experiment Design

### Model configuration

The JES ocean circulation model is based on the Regional Ocean Modeling System (ROMS), a free-surface, terrain following, and primitive equation ocean circulation model (Haidvogel et al. 2000). The model domain includes the JES and the southwestern part of Okhotsk Sea (Fig. 1). Horizontal grid spacing is approximately 3 km. The model has 41 vertical sigma layers. Realistic bottom topography data from ETOPO5 bathymetric databases of NOAA National Geophysical Data Center were interpolated on the model grid. To provide tidal mixing effect, tidal waves were propagated into the model domain across open boundaries with ten major tide and tidal current harmonic components ($M_2$, $S_2$, $O_1$, $K_1$, $N_2$, $K_2$, $P_1$, $Q_1$, $M_f$, and $M_m$) from TPXO6 (Egbert and Erofeeva 2002). Sea surface wind stress and heat fluxes across the sea surface are important for simulation of ocean circulation. The 12-hourly atmospheric surface forcing data were obtained from the European Centre for Medium-Range Weather Forecast (ECMWF) reanalysis to simulate ocean circulation. The atmospheric forcing data includes winds, surface air pressure, shortwave radiation, surface air temperature, and relative humidity. To spin up and adjust the surface velocity field in balance with the surface density field in a high resolution regional model, ocean circulation was simulated for four years before numerical experiments were conducted. Initial temperature and salinity data were provided from World Ocean Atlas 2009 and initial current and SSH data were

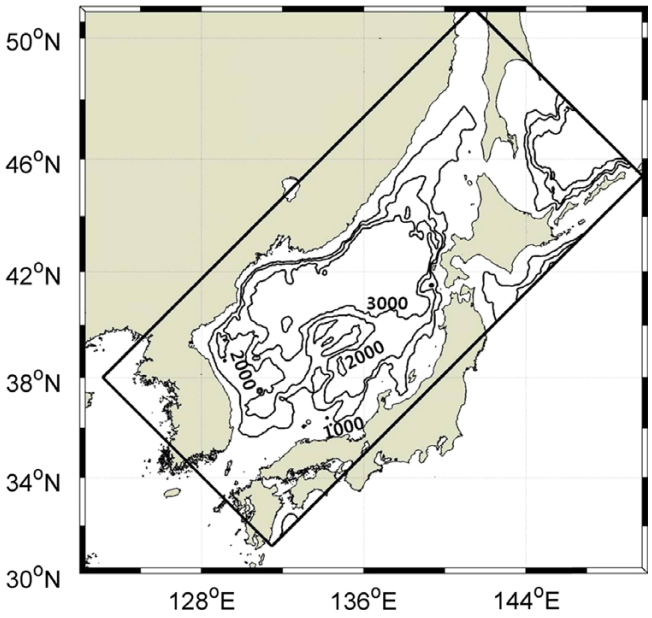


**Fig. 1.** Numerical model domain (tilted rectangle) with bottom topography for the simulation of ocean circulation in the JES. Contour lines represent 1000, 2000, and 3000 m isobaths

obtained from monthly mean data in January 1998 from a data assimilative Northwestern Pacific Regional Model with about 0.1° horizontal grid spacing (Cho et al. 2009; Seo et al. 2014). Boundary data for the four years of spin-up simulation were monthly mean data from 1998 to 2001 supplied from the same data assimilative model. After the spin-up integration, surface ocean circulation was simulated from 1998 to 2009. Open boundary data from 1998 to 2009 were also supplied from the data assimilative Northwestern Pacific Regional Model (Seo et al. 2014).

**Experiment Design**

The interannual variation of surface circulation in the JES was assumed to be induced by the following: (1) changes in atmospheric forcing conditions such as wind, air temperature and surface pressure, (2) variations in volume transport through straits, and (3) the intrinsic (internally generated) variability of surface flow. To determine which process induces the interannual variability of surface circulation, four numerical experiments, i.e., ITV, OBC, ATM, and CON, were performed (Table 1). Here, ITV, OBC, ATM, and CON represent intrinsic variability, open boundary data, atmospheric forcing, and control condition, respectively.

In the ITV experiment, atmospheric forcing and open boundary data were obtained from monthly mean data of climatology (Table 1). Interannual variability of surface circulation is induced by the intrinsic variability of the flow in the ITV experiment. In the OBC experiment, atmospheric forcing data were obtained from monthly mean data of climatology. However, open boundary data, such as temperature, salinity, and velocity at the open boundaries, were obtained from monthly data from 1998 to 2009 with interannual and seasonal variations. The interannual variability of surface circulation in the OBC experiment is induced by interannual variation of the open boundary data as well as the intrinsic variability of surface flow. In the ATM experiment, atmospheric forcing data were 12-hourly data from 1998 to 2009 while open boundary data were obtained from monthly mean climatology. The interannual variability of surface circulation in the ATM experiment is induced by interannual variation of atmospheric forcing data and intrinsic variability of the surface flow. Note that only wind forcing data were 12-hourly data of year 2005 while other atmospheric forcing data were monthly mean data of climatology in ITV and OBC experiments so that atmospheric forcing data would not have interannual variation but would have enough wind mixing at the surface layer of the ocean. In the CON experiment, atmospheric forcing data were 12-hourly data from 1998 to 2009 while open boundary data were monthly data from 1998 to 2009. The interannual variability of surface circulation in the CON experiment is induced by interannual variations of atmospheric forcing and open boundary condition as well as intrinsic variability of surface flow.

In the next section, mean field and variability of SSH, 100-m depth currents, and 100-m depth temperature are presented. The variability of variables from the four experiments

**Table 1.** Numerical experiments with intrinsic variability (ITV), interannual variation of open boundary condition (OBC), interannual variation of atmospheric forcing (ATM), and interannual variation of all factors (CON). To have enough surface wind mixing, 12-hourly wind data of year 2005 were used in ITV and OBC experiments

| Experiment | Atmospheric forcing | Open boundary data |
|---|---|---|
| ITV | Monthly Climatology (seasonal variation only) | Monthly Climatology (seasonal variation only) |
| OBC | Monthly Climatology (seasonal variation only) | Monthly mean data from 1998 to 2009 |
| ATM | ECMWF 12-hourly data from 1998 to 2009 | Monthly Climatology (seasonal variation only) |
| CON | ECMWF 12-hourly data from 1998 to 2009 | Monthly mean data from 1998 to 2009 |

**Table 2.** Estimation of relative contribution from each forcing to interannual variations of the EKWC and surface circulation in the JES. VAR[ITV] represents variance from the ITV experiment

| Experiment | Relative contribution with respect to ITV (%) | Relative contribution with respect to CON (%) |
|---|---|---|
| ITV | – | $\frac{\text{VAR[ITV]}}{\text{VAR[CON]}} \times 100$ |
| OBC | $\frac{\text{VAR[OBC]}-\text{VAR[ITV]}}{\text{VAR[ITV]}} \times 100$ | $\frac{\text{VAR[OBC]}-\text{VAR[ITV]}}{\text{VAR[CON]}} \times 100$ |
| ATM | $\frac{\text{VAR[ATM]}-\text{VAR[ITV]}}{\text{VAR[ITV]}} \times 100$ | $\frac{\text{VAR[ATM]}-\text{VAR[ITV]}}{\text{VAR[CON]}} \times 100$ |
| CON | $\frac{\text{VAR[CON]}-\text{VAR[ITV]}}{\text{VAR[ITV]}} \times 100$ | – |

is compared quantitatively in terms of root-mean-square (RMS) and variance (Hogan and Hurlburt 2005). Relative contributions of ITV, OBC, and ATM to interannual variations of surface circulation in the CON experiment are estimated in terms of variance (Metzger and Hurlburt 2001; Hogan and Hurlburt 2005) in this study (Table 2). Ratios of interannual variability in

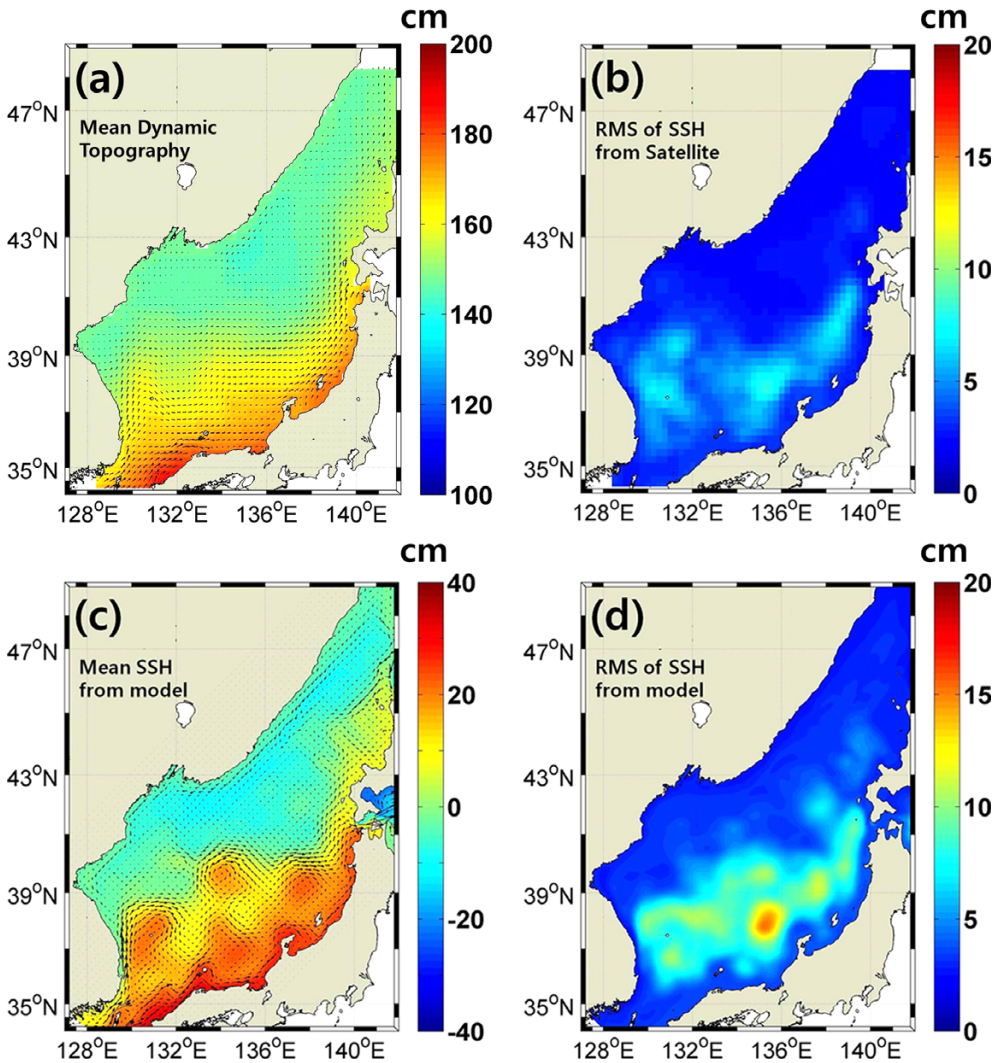


**Fig. 2.** (a) Mean SSH (cm) from long term hydrography data (Choi et al. 2004) and (b) RMS (cm) of SSH from satellite altimeter data from 1998 to 2009. (c) Mean SSH (cm) and (d) RMS (cm) of SSH from CON experiment

the OBC, ATM, and CON experiments relative to that in the ITV experiment are also estimated (Table 2).

## 3. Results

### Mean SSH and variability

The surface mean geostrophic current was estimated from the distribution of mean dynamic topography (or mean SSH) from long-term mean hydrography data (Fig. 2a). After the EKWC separates from the coast, it flows northeastward along the Polar Front toward the Tsugaru Strait. Because the EKWC meanders and deviates from the mean path year to year, RMS of SSH is high around the mean path of the EKWC (Fig. 2b). RMS of SSH was estimated from satellite altimeter data from 1998 to 2009, which had been low-pass filtered with filter-length of 6 weeks (Ducet et al. 2000). Distribution of the mean SSH and the mean surface current from the CON experiment was similar to that obtained from the long-term mean hydrography data (Fig. 2c). The RMS of SSH from the CON experiment was high in the Ulleung Basin and the Yamato Basin, with a maximum at 135°E, 37.5°N (Fig. 2d). RMS of SSH from monthly mean data of the CON experiment was larger than that obtained from the satellite altimeter data.

RMSs of SSH from ITV, OBC, ATM, and CON experiments were compared (Fig. 3). RMS of SSH was relatively large in the southern part of the JES in all four experiments. Distribution of the SSH variability from the ITV experiment was similar to that obtained from satellite observation: RMSs of SSH was relatively high in the northwest of Ulleung Island and in the southwest of the Tsugaru Strait with a maximum at the southern Yamato Basin (135°E, 38°N) in both observation and simulation. This implies that the interannual variability of the surface ocean circulation can be intrinsically modulated without interannual variability caused by external forcing such as atmospheric forcing or open boundary data. However, the model simulation had excessively large RMS of SSH over the Yamato Rise and did not reproduce relatively high RMS of SSH at 131°E, 39.5°N (Figs. 2b and 3a). When the interannual variation of the open boundary data was added in the OBC experiment, the RMS of SSH was enhanced in the southern part of the JES, especially at the Yamato Basin (Fig. 3b). When the interannual variation of the atmospheric variability was added in the ATM experiment, the RMS of SSH increased in the Ulleung Basin (Fig. 3c).

Relative contribution of controlling factors to the interannual

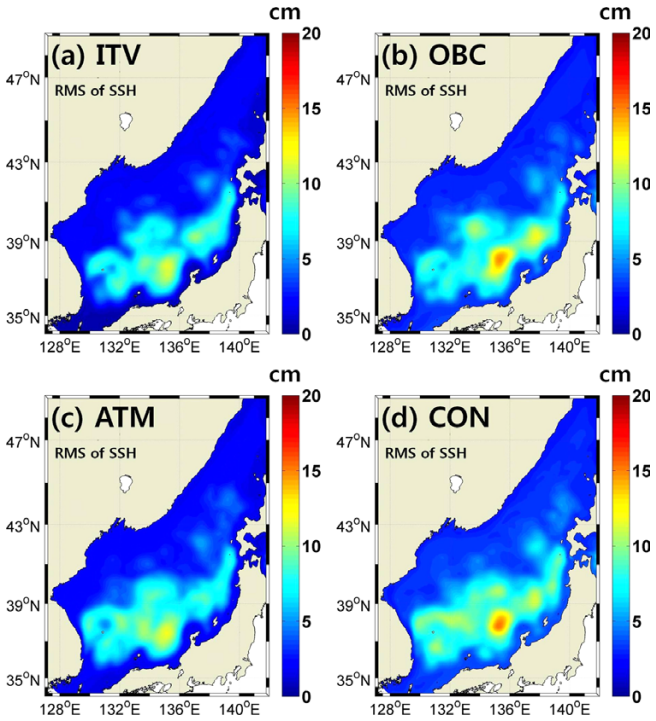


**Fig. 3.** RMS of sea surface height (cm) in (a) ITV, (b) OBC, (c) ATM, and (d) CON experiments

**Table 3.** Estimation of relative contribution from each forcing to interannual variation of sea surface height in the JES. VAR represents variance ($cm^2$) of sea surface height in each experiment

| Experiment | VAR ($cm^2$) | Relative contribution with respect to ITV (%) | Relative contribution with respect to CON (%) |
|---|---|---|---|
| ITV | 7.56 | – | 40.89 |
| OBC | 15.29 | 102.25 | 41.81 |
| ATM | 10.18 | 34.66 | 14.17 |
| CON | 18.49 | 144.58 | – |

variation of SSH was estimated in terms of variance (Table 2). Average variances of SSH in the ITV, OBC, ATM, and CON experiments were 7.56 $cm^2$, 15.29 $cm^2$, 10.18 $cm^2$, and 18.49 $cm^2$, respectively (Table 3). The variance of SSH from the OBC experiment was larger than that obtained from the ATM experiment.

Variances from the OBC, ATM, and CON experiments included variance from the ITV experiment because the intrinsic variability was embedded in the OBC, ATM, and CON experiments. The addition of interannual variability from open boundary data to the system increased about 102% in variance relative to that in the ITV experiment. However, the addition of interannual variability from atmospheric forcing

to the system increased about 35% in variance relative to that in the ITV experiment.

If the variance from the CON experiment is a combination of contributions from ITV, OBC, and ATM forcing, the relative contribution can be estimated with respect to variance in the CON experiment. The interannual variability from the intrinsic variability, open boundary data, and atmospheric forcing contributed about 41%, 42%, and 14%, respectively. The relatively large contribution of OBC to SSH variability can be misleading because the large SSH variability in the OBC experiment is related to uniform basin-wide oscillation rather than interannual variation of surface circulation. This will be discussed in section 4.

**Surface currents and their variabilities at 100-m depth**

Mean currents for 12 years were calculated for each experiment. Current speeds were relatively large (> 0.20 m/s) along the main paths of the EKWC, Tsushima Warm Current (TWC), Primorye Cold Current and North Korea Cold Current (Fig. 4). In the southern part of the JES, the EKWC flows from the Korea Strait to 37°N along the east coast of Korea and separates from the coast to the northeast. However, the TWC flows along the Japanese coast from the Korea Strait to Oki Spur and separates from the coast to the north (Fig. 4).

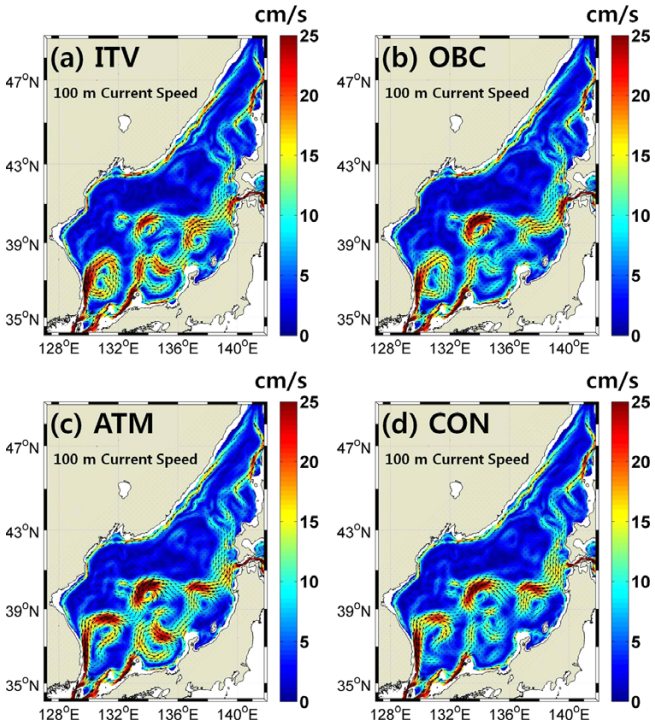


**Fig. 4.** Mean current (cm/s) at 100-m depth in (a) ITV, (b) OBC, (c) ATM, and (d) CON experiments

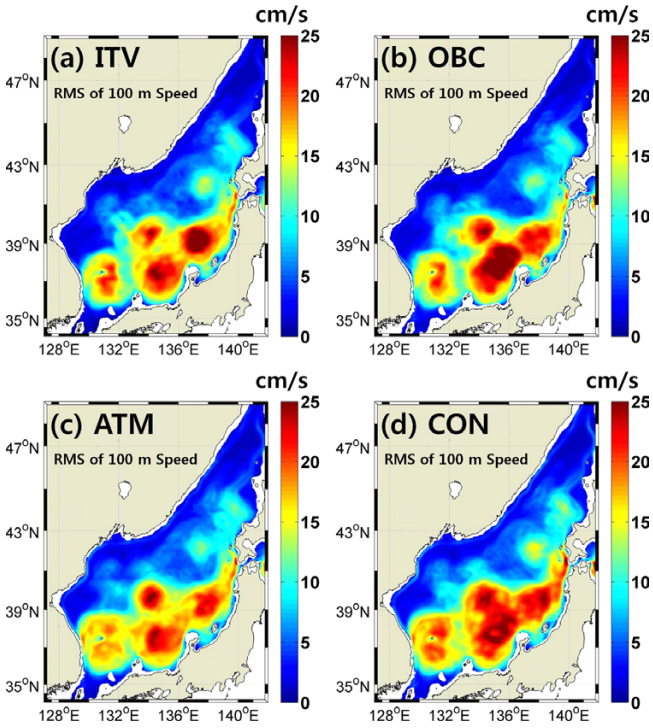


**Fig. 5.** RMS of 100-m depth current speed (cm/s) for (a) ITV, (b) OBC, (c) ATM, and (d) CON experiments

Surface currents flow northeastward in the Yamato Basin and converge in the southwest of the Tsugaru Strait to flow through the strait. In the northern part of the JES, the Primorye Cold Current and the North Korea Cold Current flow southwestward along the coast.

RMS of the nonseasonal current anomaly was calculated at each grid point. Here, the nonseasonal current anomaly was obtained by subtracting the long-term (12 years) mean monthly current from the time series of monthly current. Thus, the time series of the monthly nonseasonal current anomaly do not have a mean seasonal cycle. It was found that spatial patterns for the RMS of the nonseasonal current anomaly were similar for all experiments (Fig. 5). The RMS of the monthly nonseasonal current anomaly was large in the Ulleung Basin and the Yamato Basin. Average variances of the nonseasonal current anomaly in ITV, OBC, ATM, and CON experiments were 60 $cm^2/s^2$, 72 $cm^2/s^2$, 66 $cm^2/s^2$, and 88 $cm^2/s^2$, respectively (Table 4). When the interannual variability from open boundary data was added to the system (OBC experiment), the variance of the nonseasonal current anomaly increased about 21% relative to that in the ITV experiment. The variability of surface current was enhanced in the northwest of the Noto Peninsular. When the interannual variability of atmospheric

**Table 4.** Estimation of relative contribution from each forcing to nonseasonal variation of EKWC and surface circulation in the JES. VAR represents variance ($cm^2/s^2$) of current speed in each experiment

| Experiment | VAR ($cm^2/s^2$) | Relative contribution with respect to ITV (%) | Relative contribution with respect to CON (%) |
|---|---|---|---|
| ITV | 60.06 | – | 67.97 |
| OBC | 72.42 | 20.58 | 13.99 |
| ATM | 66.42 | 10.59 | 7.20 |
| CON | 88.36 | 47.12 | – |

forcing was added to the model (ATM experiment), the variance of the nonseasonal current anomaly increased about 11% relative to that in the ITV experiment. The region of high variability was also expanded in the Ulleung Basin.

If the variance of the nonseasonal current anomaly from the CON experiment is a combination of contributions from the nonseasonal variability of ITV, OBC, and ATM experiments, the relative contribution can be estimated with respect to ocean current variance from the CON experiment. The interannual variability from intrinsic variability, open boundary data, and atmospheric forcing contributed to the interannual variability of surface current by about 68%, 14%, and 7%, respectively (Table 4).

### Temperature variability at 100-m depth

Distribution of mean temperature at 100-m depth is affected by warm water provided to the southern JES and the meandering pattern of surface current (Fig. 6). There is a strong temperature gradient between 7°C and 10°C isotherms, which separates the southern warm water region and cold water region at 100-m depth in the model. Currents along the boundary between the warm and cold water regions are stronger and wider than other currents (Fig. 4). Fluctuations of the 10°C isotherm at 100-m depth are related to the meandering of mean currents such as the EKWC and TWC.

When the interannual variation of the open boundary data was included in model forcing (OBC experiment), the spatial pattern of the mean temperature at 100-m depth was similar to that in the ITV model. However, when the interannual variability of the atmospheric forcing was added to model forcing (ATM and CON experiments), the warm water region expanded slightly to the north relative to that in the ITV and OBC experiments while the distance between the 5°C isotherm and 10°C isotherm was shortened.

RMS of the 100-m depth temperature was calculated at each grid point. It was large around the Ulleung Basin (Fig. 7). Average variances of the 100-m depth temperature in the

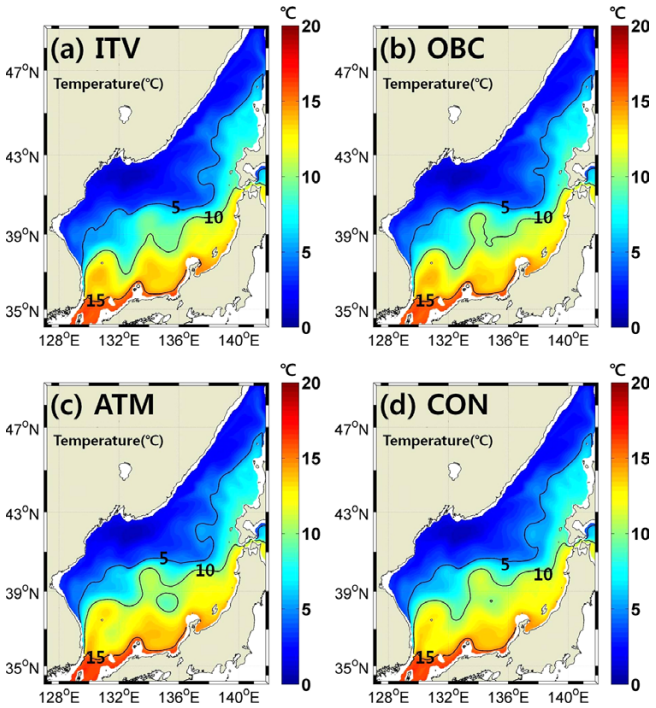


**Fig. 6.** Mean temperature (°C) at 100-m depth from in ITV, (b) OBC, (c) ATM, and (d) CON experiments

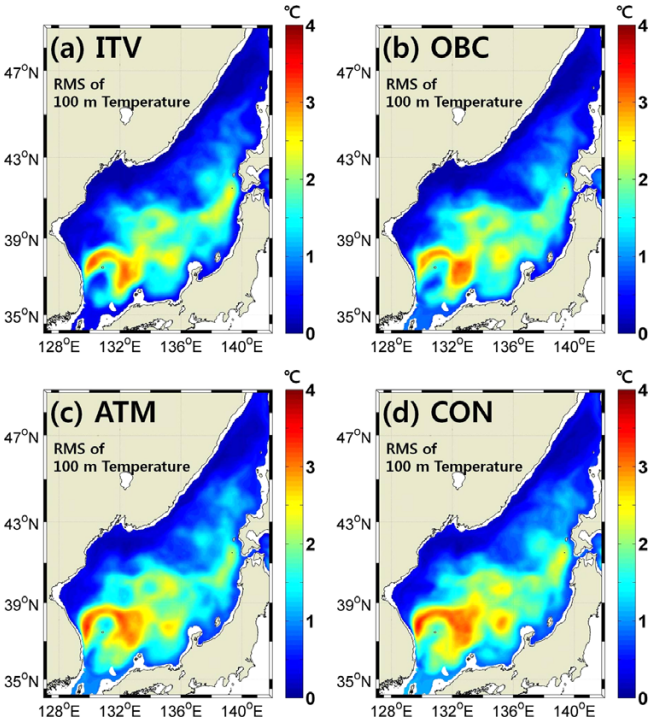


**Fig. 7.** RMS of 100-m depth temperature (°C) in (a) ITV, (b) OBC, (c) ATM, and (d) CON experiments

**Table 5.** Estimation of relative contribution from each forcing to interannual variation of 100-m depth temperature (°C) in the JES. VAR represents variance ($°C^2$) of 100-m depth temperature in each experiment

| Experiment | VAR ($°C^2$) | Relative contribution with respect to ITV (%) | Relative contribution with respect to CON (%) |
|---|---|---|---|
| ITV | 0.64 | – | 59.81 |
| OBC | 0.80 | 25.00 | 14.95 |
| ATM | 0.89 | 39.06 | 23.36 |
| CON | 1.07 | 67.19 | – |

ITV, OBC, ATM, and CON experiments were 0.64°$C^2$, 0.80°$C^2$, 0.89°$C^2$, and 1.07°$C^2$, respectively (Table 5). When the interannual variation of the open boundary data was included in the external forcing (OBC experiment), average variance increased about 25% relative to that in the ITV experiment while the spatial pattern was only changed slightly (Fig. 7b). As the interannual variability of the atmospheric forcing was added to the external forcing (ATM experiment), average variance increased about 39% relative to that in the ITV experiment and the region of high variability was expanded around the Ulleung Basin due to the interannual path change of the EKWC. Distribution of the mean temperature and its variability at 100-m depth indicate that the warm water region with high meandering activity of the flow can expand to the north by interannual variation of the atmospheric forcing (Figs. 6 and 7).When the relative contribution of each factor to interannual variation of the 100-m depth temperature (CON experiment) was determined based on variances, it was about 60%, 15%, and 23% in the ITV, OBC, and ATM experiments, respectively (Table 5). This variance analysis suggests that the interannual variation of the 100-m depth temperature is induced mostly by intrinsic variability (ITV) of the flow in the JES.

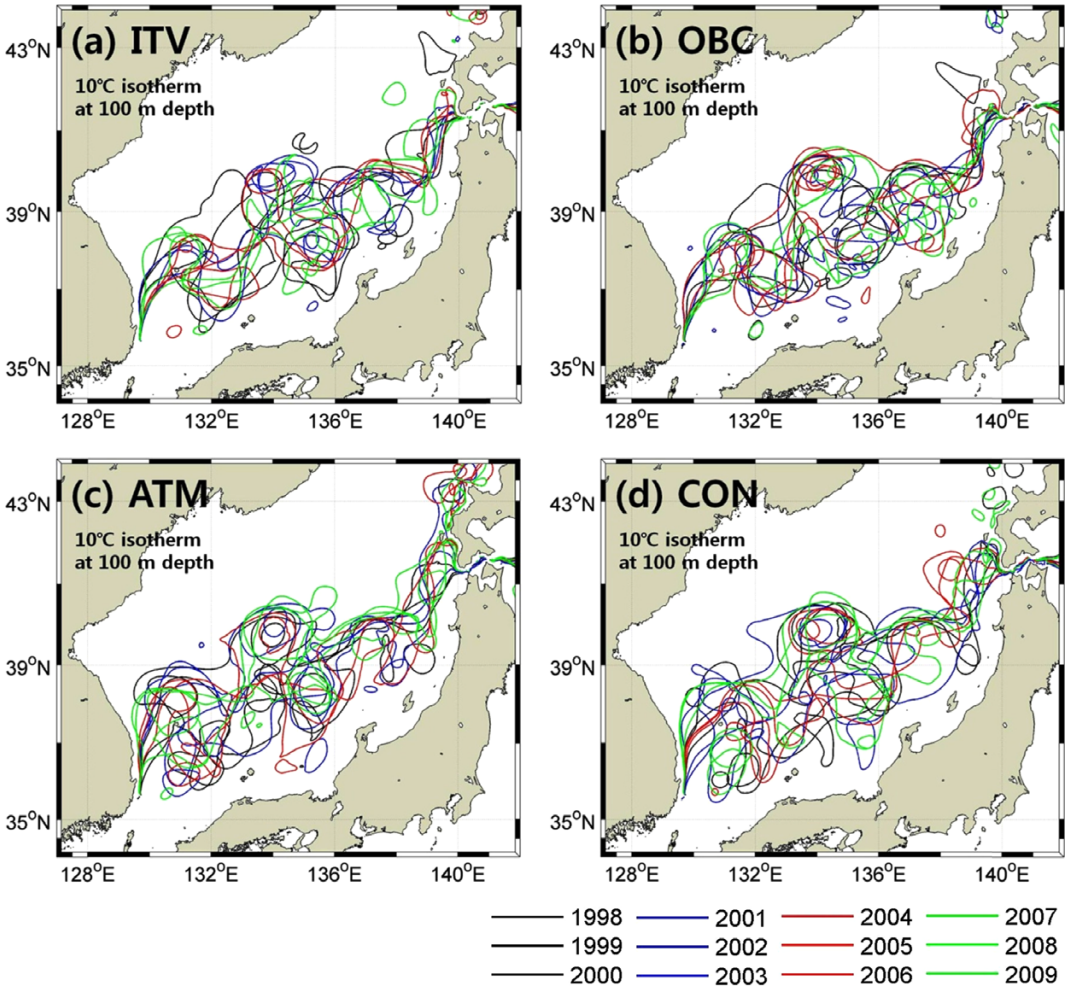


**Fig. 8.** Horizontal distribution of 10°C isotherms at 100-m depth in (a) ITV, (b) OBC, (c) ATM, and (d) CON experiments in August from 1998 to 2009

**Variation of the EKWC main path**

The main path of the EKWC (Fig. 4) follows approximately the 10°C isotherm at 100-m depth (Fig. 6). Spatial location of the 10°C isotherm at 100-m depth is assumed to represent the main path of the EKWC in this section. To visualize the interannual path variation of the EKWC, 10°C isotherms at 100-m depth were plotted for August in each year (Fig. 8). Compared to the annual mean location of the 10°C isotherm at 100-m depth (mean path of the EKWC) in Fig. 6, locations of the 10°C isotherm at 100-m depth move farther north with large meandering in August (Fig. 8). This implies that the warm water region expands to the north and the meandering of the EKWC is prominent in August (Fig. 8).

When only the mean seasonal cycle of the open boundary data and atmospheric forcing was provided to the model (ITV experiment), the EKWC meandered in the southern warm water region and the main path changed year to year. The number of waves with the current meandering was about four to five from the east coast of Korea to the Tsugaru Strait. When interannual variability of the open boundary data was included (OBC experiment), the amplitude of the EKWC meandering increased in the middle of the southern JES. However, the path of the EKWC near the east coast of Korea and in the west of the Tsugaru Strait seemed to be clamped in both ITV and OBC experiments. Once the interannual variation of the atmospheric forcing was introduced into the model (ATM and CON experiments), the separation location and path of the EKWC widely varied each year in the southwestern JES. The first meandering envelop of the EKWC in the southwestern JES expanded farther north in some years, which might be related to the relative large variability of the 100-m depth temperature around Ulleung Basin (Fig. 7) in the ATM and CON experiments.

**Variation of surface kinetic energy**

Mean kinetic energy ($(u^2 + v^2) / 2$) at 5-m depth was about 0.029 $m^2/s^2$ and that at 100-m depth was 0.019 $m^2/s^2$ in the CON experiment. The kinetic energy at 5- and 100-m depths had seasonal variation. It was the smallest in the winter (February and March) but was the largest in the summer (August and September) in all experiments. Mean kinetic energy in the summer (winter) was about 0.037 (0.022) $m^2/s^2$ with RMS of 0.0047 (0.0028) $m^2/s^2$ at 5-m depth in the CON experiment. These figures indicate that the surface circulation is stronger in the summer and its interannual and intra-seasonal variabilities are also more prominent in the summer.

To examine the nonseasonal variation of surface kinetic energy, the mean seasonal variation was removed from the time series of kinetic energy at 5- and 100-m depths (Fig. 9). The surface kinetic energy had interannual variation featuring a time scale of about 4 years. It also showed intra-seasonal variability. RMSs of the nonseasonal surface kinetic energy

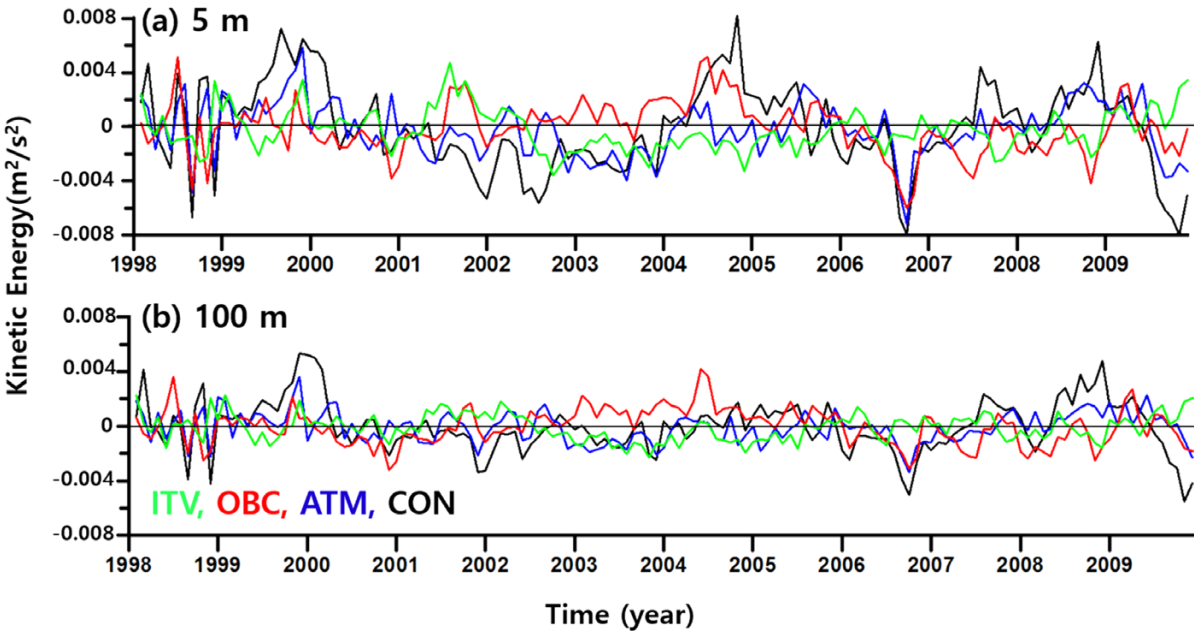


**Fig. 9.** Nonseasonal variation of kinetic energy at 5- and 100-m depth in ITV (green line), OBC (red line), ATM (blue line), and CON (black line) experiments from 1998 to 2009

at 5-m depth were 0.0032 $m^2/s^2$ in the CON experiment, 0.0019–0.0020 $m^2/s^2$ in the ATM and OBC experiments, and 0.0015 $m^2/s^2$ in the ITV experiment.

For the CON experiment, the mean kinetic energy was relatively high in September 1999 and September 2004. It was relatively low in September 2006 and September 2009. When the mean kinetic energy was relatively high (low), the gradient of both SSH and subsurface temperature across the main path of the EKWC were stronger (weaker) and the meandering amplitude of the EKWC was larger (smaller).

## 4. Discussion

The distribution of SSH is closely related to the pattern of sea surface circulation in the JES (Figs. 2 and 4). To understand the spatial pattern and temporal time scale of the interannual variability of surface circulation, EOF analysis was performed on the SSH data from satellite altimeter observation and numerical experiments. Both observed and simulated SSH were analyzed from 1998 to 2009. Linear trend and mean seasonal variation were removed before the EOF analysis (Choi et al. 2004).

### EOF analysis of the observed SSH

The EOF first mode accounted for 30.3% of the total variance in nonseasonal variability from satellite altimeter observation. The first EOF was positive in the entire domain. It was relatively large in the north of Ulleung Island and along the Yamoto Basin (Fig. 10a). The first mode of the SSH variability is related to the intensification of the EKWC along the east coast of Korea as well as basin-wide uniform oscillations of sea level (Choi et al. 2004, 2012; Lee and Niiler 2010). When the amplitude time series of the first mode is positive, the SSH gradient across the EKWC increased along the east coast of Korea. The intensified EKWC reaches about 40°N in the northwest JES (Fig. 11a of Choi et al. 2012). The second mode of the SSH variability accounted for 9.6% of the total variance. It is related to the meandering of the EKWC (Fig. 10b). When the amplitude time series of the second mode is negative, a large meandering pattern of the EKWC (Fig. 2a) appears in the southern JES (Naganuma 1973; Fig. 13b of Choi et al. 2004).

### The first EOF mode of the simulated SSH

The first EOFs of SSH anomalies from the ITV and ATM experiments had negative and positive regions. They appeared alternatively from the Korea Strait to the Tsugaru Strait in the southern warm water region (Fig. 11a and c). The alternating pattern of the positive and negative regions is related to the meandering of the EKWC and eddies. The first EOFs of SSH anomalies from the OBC and CON experiments had positive background values with negative and positive cores in the warm water region (Fig. 11b and d). The positive background value is related to basin-wide uniform oscillations with a time scale of 2–6 months (Choi et al. 2004; Kim and Fukumori 2008).

The amplitude time series of the first EOF mode from satellite observed SSH (Fig. 12a) has intra-seasonal variations with a time scale of 4 and 15 months as well as the interannual variation with a time scale of 3 years (Fig. 13a). The amplitude

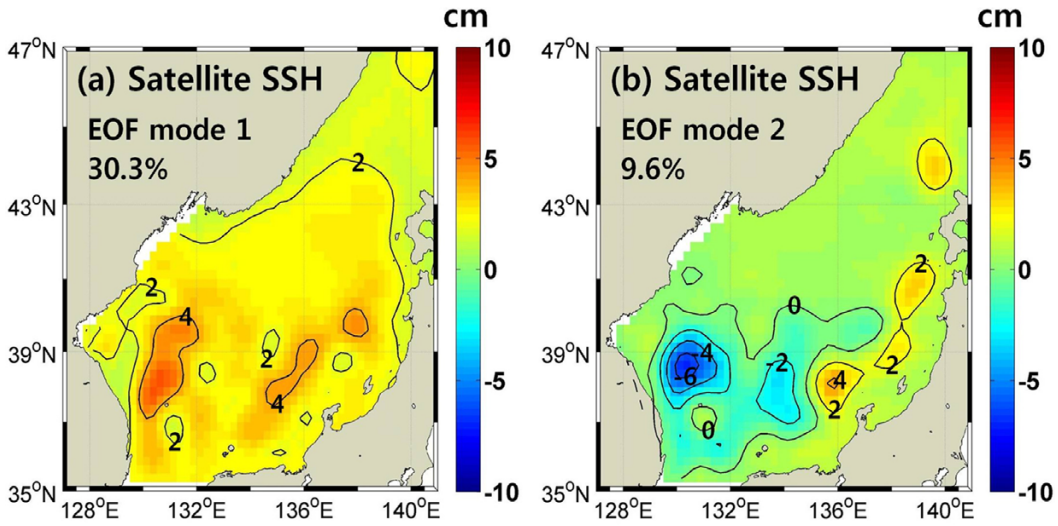


**Fig. 10.** The first and second EOFs of nonseasonal SSH obtained from satellite observation from 1998 to 2009

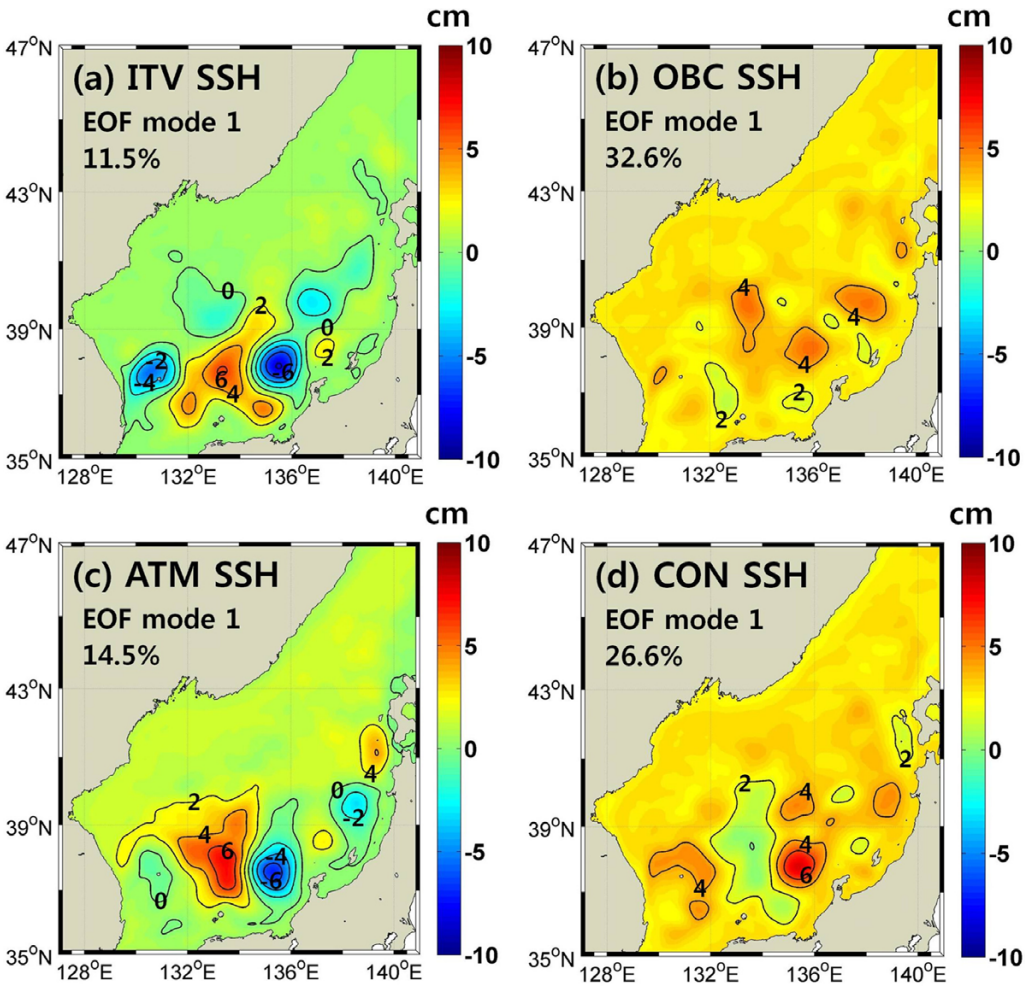


**Fig. 11.** The first EOFs of nonseasonal SSH in (a) ITV, (b) OBC, (c) ATM, and (d) CON experiments

time series of the first EOF mode from the OBC experiment has intra-seasonal variations with about 5–15 months periods as well as the interannual variation with about 3 years period (Fig. 13b). However, the amplitude time series of the CON experiment has intra-seasonal variations characterized by about 5, 10, and 15 month periods (Fig. 13c). The amplitude time series of the first EOF mode from the ITV and ATM experiments have interannual variations featuring a time scale of approximately 2–4 years and relatively small intra-seasonal variability. The first EOF modes of SSH anomalies obtained from the numerical simulations indicate that near uniform basin-wide oscillations characterized by a timescale of 5–15 months are related to variations of open boundary data, i.e., inflow and outflow transports, in the OBC and CON experiments (Kim and Fukumori 2008).

**The second EOF mode of the simulated SSH**

The second EOF mode accounted for 10.3%, 8.4%, 10.7%, and 7.9% of total variance in nonseasonal SSH variability from the ITV, OBC, ATM and CON experiments, respectively. The second EOFs have an alternating pattern of positive and negative cores in the southern JES in all experiments (Fig. 14). This represents the path change or meandering of the EKWC (Choi et al. 2004, 2012). The spatial patterns of the second EOFs from numerical simulations were similar to that of the second EOF from satellite observation. However, numerical simulations did not reproduce the negative core in the western JES (130.5°E, 38.5°N). In the ITV experiment, spatial pattern of the second EOF of the satellite-observed SSH was reproduced in the warm water region without interannual variations in external forcing. This implies that the EKWC path change or meandering can be modulated

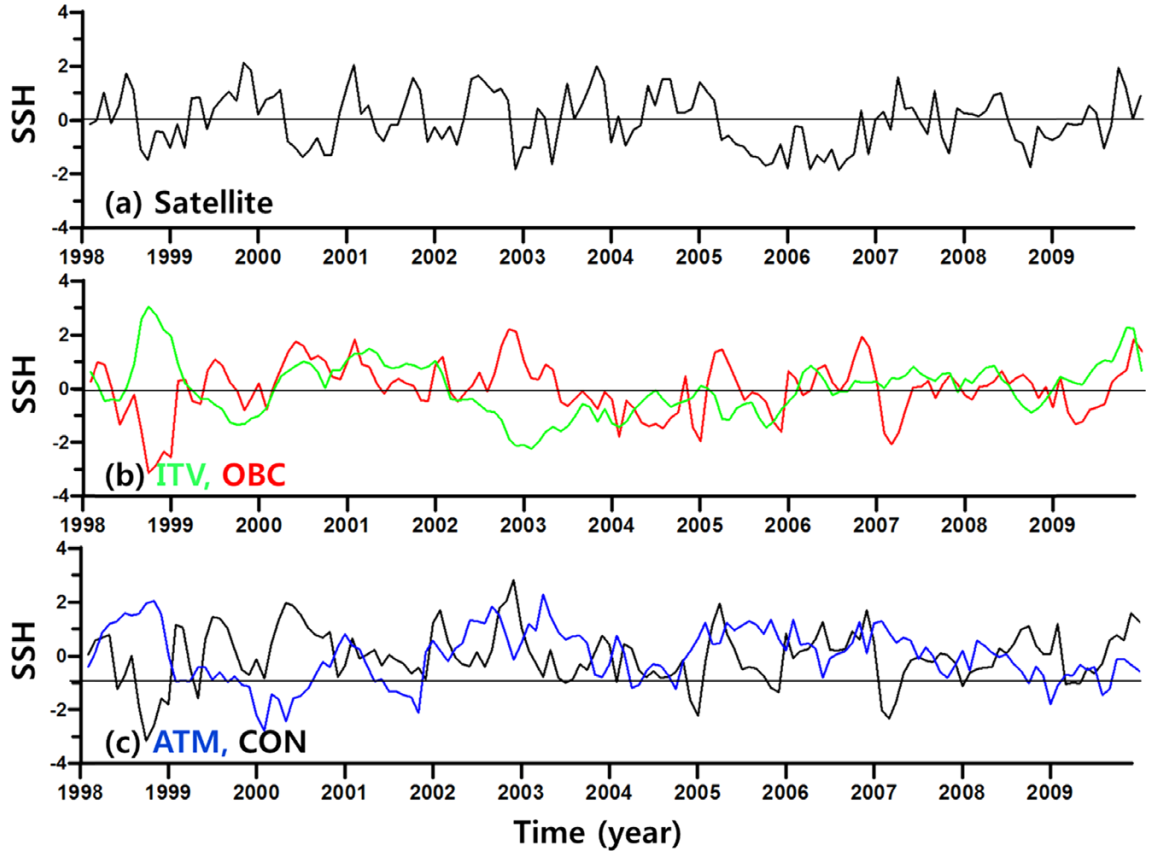


**Fig. 12.** Normalized amplitude time series of the first EOF mode of nonseasonal SSH in (a) satellite observation, (b) ITV and OBC experiments, and (c) ATM and CON experiments

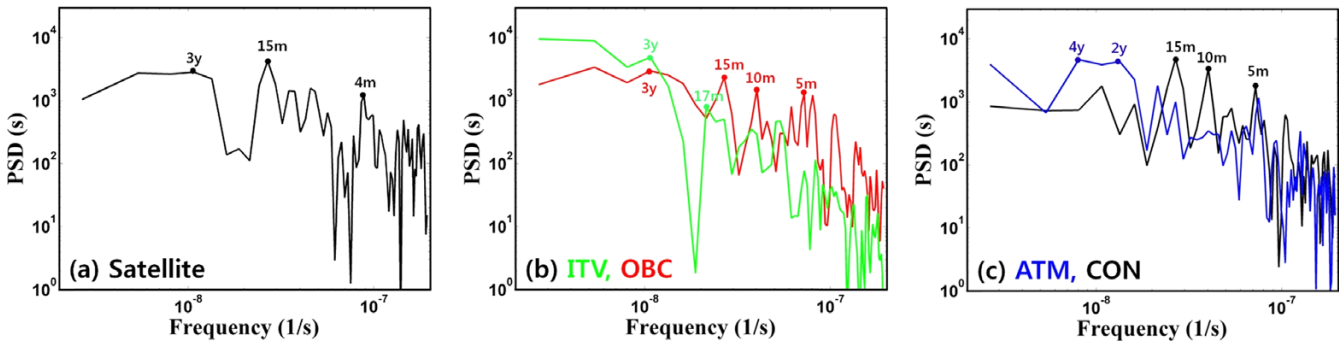


**Fig. 13.** Power spectrum from the normalized first mode amplitude time series of nonseasonal SSH: (a) satellite, (b) ITV and OBC, (c) ATM and CON experiments. PSD, y, and m stand for power spectral density, year, and month, respectively

solely by the intrinsic variability. The OBC, ATM, and CON experiments might have inherited the intrinsic interannual variability of the surface flow from the ITV experiment. There are three to four positive and negative cores from the Korea Strait to the Tsugaru Strait. The wave length of the meander is expected to be about 250–330 km as shown in Fig. 14 (Moriyasu 1972).

The amplitude time series of the second EOF mode from satellite observed SSH has interannual variation with a period longer than 2 years (Fig. 15). The amplitude time series of the second EOF modes from the ITV, OBC, ATM, and CON experiments have interannual variations with about 2–4 years periods in addition to intra-seasonal variability (Fig. 16). The spatial pattern and amplitude time series of the second

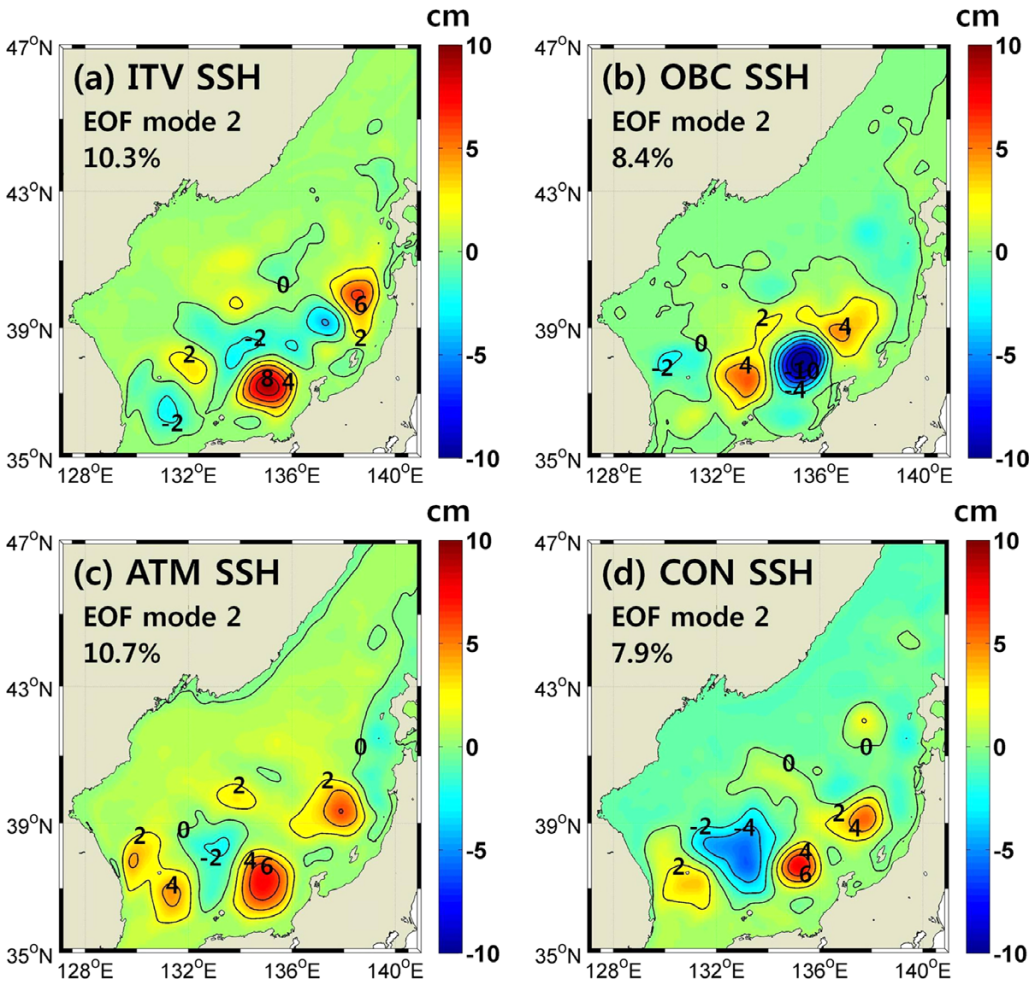


**Fig. 14.** Second EOFs of nonseasonal SSH in (a) ITV, (b) OBC, (c) ATM, and (d) CON experiments

EOF mode indicate that the low frequency path changes of the EKWC with periods of 2–4 years and wavelength of 250–330 km are related to intrinsic variations of the EKWC (Figs. 14a and 15b).

**The quasi-biennial variability in the Yamato Basin**

The second EOFs of SSH from the ITV and OBC experiments have large (> 8 cm) cores in the Yamato Basin (135.5°E, 38.0°N). Its amplitude time series has interannual variability characterized by a temporal time scale of approximately 2–3 years (Figs. 15 and 16). The second EOFs of SSH from the ATM and CON experiments also have cores (> 6 cm) in the Yamato Basin (135.5°E, 38.0°N) because the ATM and CON experiments inherit characteristics of the ITV experiment. The second EOF of SSH from satellite observation also has a core in the Yamato Basin. Its amplitude time series has interannual variability characterized by a temporal time scale of approximately 2 years (Figs. 15a and 16a). The low frequency variability of SSH in the Yamato Basin has been known as quasi-biennial variability (Hirose and Ostrovskii 2000; Choi et al. 2004). Hirose and Ostrovskii (2000) suggested that the quasi-biennial variability in the Yamato Basin is modulated by intrinsic nonlinearity of the flow and intra-seasonal wind variation. The cause of high SSH variability in the Yamato Basin was not presented in the study of Choi et al. (2004). In this study, the quasi-biennial variability of SSH in the Yamato Basin was found to be caused by ITV (Fig. 3a). It was enhanced by the interannual variability in the OBC experiment (Fig. 3b). The physical mechanism to explain how signals from OBC are transferred to the Yamato Basin and enhance the quasi-biennial variability needs to be investigated in the future.

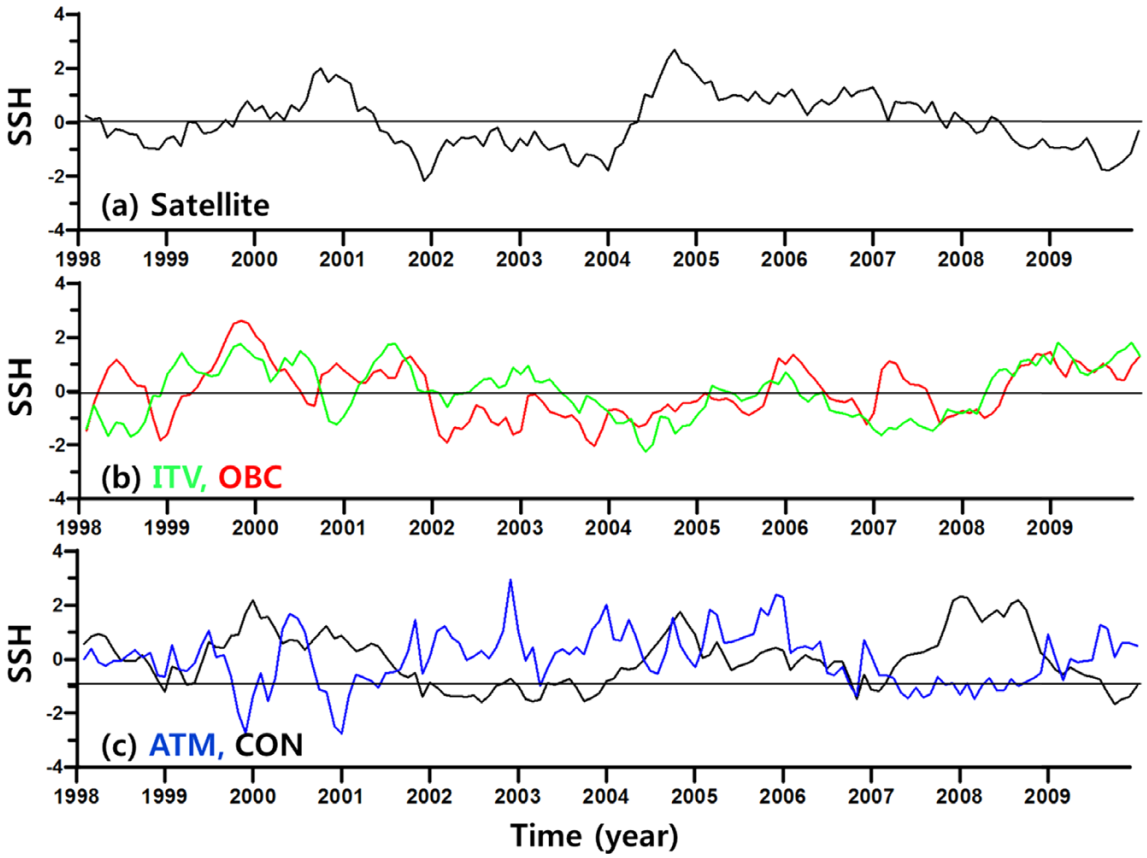


**Fig. 15.** Normalized amplitude time series of the second EOF mode of nonseasonal SSH in (a) satellite observation, (b) ITV and OBC experiments, and (c) ATM and CON experiments

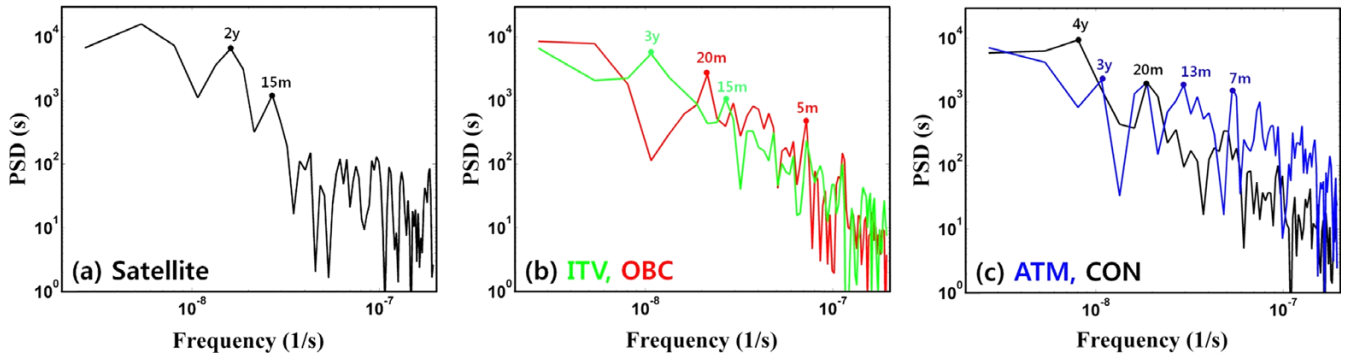


**Fig. 16.** Power spectrum from the normalized second mode amplitude time series of nonseasonal SSH: (a) satellite, (b) ITV and OBC, (c) ATM and CON experiments. PSD, y, and m stand for power spectral density, year, and month, respectively

**Other external forcing and intrinsic variability**

Not all external forcing factors were examined in this study. Winter time cooling in the northern JES may affect subsurface circulation along the northwestern boundary of the JES, which in turn can intensify the Primorye Current and the North Korea Cold Current along the northwestern boundary of the JES and modulate variations in the separation latitude of the EKWC (Isoda 1999; Kim et al. 2009). Hirose and Ostrovskii (2000) argued that weak summer monsoon wind stress curl field can excite the quasi-biennial variability. Choi et al. (2009) claimed that nonseasonal variation of zonal wind stress over the southwestern JES can affect the separation location of the EKWC and its meandering path.

Lee (1999) studied self-excited and internally generated

variability of the EKWC using numerical simulations and suggested that the likely source of the intrinsic variability is barotropic instability. Jiang et al. (1995), Hirose and Ostrovskii (2000), and Hogan and Hurlburt (2005) also suggested that intrinsic nonlinearity is a possible cause of interannul variations in the surface circulation in the JES.

## 5. Summary

Intrinsic (internally generated) variability is found to be the dominant factor that produces interannual variations in surface circulation and meandering path of the EKWC in the southern JES. Interannual variations in OBC and ATM can augment interannual variation in surface circulation. The interannual variation of ATM changes the separation latitude of EKWC and increases the variability of surface circulation in the Ulleung Basin. The interannual variation of OBC enhances low-frequency variability in surface circulation and eddies in the Yamato Basin. Spatial length-scale of the meandering EKWC path was about 250–330 km and the temporal time scale of interannual variation was about 2–4 years. This study suggests that accurate estimation of initial conditions using data assimilation is a primary factor for accurate long-term prediction of ocean circulation in the JES while the accuracy of external forcing such as OBC and ATM plays a secondary role.

## Acknowledgements

This work was supported by Kunsan National University's long-term overseas research program for faculty members in 2014. This research was part of the project entitled "Development of Korea Operational Oceanographic System (KOOS), Phase 2" and "Environmental Risk Assessment of Microplastics in the Marine Environment" funded by the Ministry of Oceans and Fisheries, Republic of Korea. This research was also part of the project entitled "Study on developing sea surface current map in the neighboring seas of Korea" funded by the Korea Hydrographic and Oceanographic Agency (KHOA). Numerical model simulations using supercomputer were made possible with a grant from the KHOA.

## References

Cho YK, Seo GH, Choi BJ, Kim S, Kim YG, Youn YH, Dever EP (2009) Connectivity among straits of the northwest Pacific marginal seas. J Geophys Res **114**:C06018. doi:10.1029/2008JC005218

Choi BJ, Haidvogel DB, Cho YK (2004) Nonseasonal sea level variations in the Japan/East Sea from satellite altimeter data. J Geophy Res **109**:C12028. doi:10.1029/2004JC002387

Choi BJ, Haidvogel DB, Cho YK (2009) Interannual variation of the Polar Front in the Japan/East Sea from summertime hydrography and sea level data. J Marine Syst **78**:351–362

Choi BJ, Byun DS, Lee KH (2012) Satellite-altimeter-derived East Sea surface currents: estimation, description and variability pattern. J Korean Soc Oceanogr **17**:225–242

Condron A, Renfrew IA (2013) The impact of polar mesoscale storms on northeast Atlantic Ocean circulation. Nat Geosci **6**:34–37

Ducet N, Le Traon P-Y, Reverdin G (2000) Global high resolution mapping of ocean circulation from TOPEX/Poseidon and ERS-1 and -2. J Geophys Res **105**:19477–19498

Egbert GD, Erofeeva SY (2002) Efficient inverse modeling of barotropic ocean tides. J Atmos Ocean Tech **19**:183–204

Haidvogel DB, Arango HG, Hedstrom K, Beckmann A, Malanotte-Rizzoli P, Shchepetkin AF (2000) Model evaluation experiments in the North Atlantic Basin: simulations in nonlinear terrain following coordinates. Dynam Atmos Oceans **32**:239–281

Hirose N, Ostrovskii AG (2000) Quasi-biennial variability in the Japan Sea. J Geophys Res **105**:14011–14027

Hogan PJ, Hulbert HE (2005) Sensitivity of simulated circulation dynamics to the choice of surface wind forcing in the Japan/East Sea. Deep-Sea Res Pt II **52**:1464–1489

Holloway G, Sou T, Eby M (1995) Dynamics of circulation of the Japan Sea. J Mar Res **53**:539–569

Isoda Y (1999) Cooling-induced current in the upper ocean of the Japan Sea. J Oceanogr **55:**585–596

Jiang S, Jin FL, Ghil M (1995) Multiple equilibria, periodic, and aperiodic solutions in a wind-driven, double-gyre, shallow-water model. J Phys Oceanogr **25**:764–786

Kim K, Cho YK, Choi BJ, Kim YG, Beardsley RC (2002) Sea level variability at Ulleung Island in the East (Japan) Sea. J Geophys Res **107**(C3):3015. doi:10.1029/2001JC000895

Kim SB, Fukumori I (2008) A near uniform basin-wide sea level fluctuation over the Japan/East Sea: a semienclosed sea with multiple straits. J Geophys Res **113**:C06031. doi:10.1029/2007JC004409

Kim YH, Chang KI, Park JJ, Park SK, Lee SH, Kim YG, Jung KT, Kim K (2009) Comparison between a reanalyzed product by 3-dimensional variational assimilation technique and observations in the Ulleung Basin of the East/Japan Sea. J Marine Syst **78**:249–264

Lee DK, Niiler P (2010) Surface circulation in the southwestern Japan/East Sea as observed from drifters and sea surface height. Deep-Sea Res Pt I **57**:1222–1232

Lee SK (1999) Self-excited variability of the East Korean Warm

Current: a quasi-geostrophic model study. J Korean Soc Oceanogr **34**:1–21

Meinvielle M, Brankart JM, Brasseur P, Barnier B, Dussin R, Verron J (2013) Optimal adjustment of the atmospheric forcing parameters of ocean models using sea surface temperature data assimilation. Ocean Sci **9**:867–883

Metzger EJ, Hurlburt HE (2001) The nondeterministic nature of Kuroshio penetration and eddy shedding in the South China. J Phys Oceanogr **31**:1712–1732

Moriyasu S (1972) The Tsushima Current. In: Stommel H, Yoshida K (eds) Kuroshio: its physical aspects, University of Tokyo Press, Tokyo, pp 353–369

Naganuma K (1973) On discussions on the existence of the Third-Branch of the Tsushima current. Jpn Sea Reg Fish Res Lab **266**:1–3 (in Japanese)

Nonaka M, Sasai Y, Sasaki H, Taguchi B, Nakamura H (2016) How potentially predictable are midlatitude ocean currents? Sci Rep **6**:20153. doi:10.1038/srep20153

Seo GH, Cho YK, Choi BJ (2014) Variations of heat transport in the northwestern Pacific marginal seas inferred from high-resolution reanalysis. Prog Oceanogr **121**:98–108

Wolfe C, Cessi P, Cornuelle B (2017) An intrinsic mode of interannual variability in the Indian Ocean. J Phys Oceanogr **47**:701–719